FM Noise Waveforms Optimized According to a Temporal Template Error (TTE) Metric

Charles A. Mohr, Shannon D. Blunt
Radar Systems Lab (RSL), University of Kansas, Lawrence, KS

***Abstract*—It has recently been shown that a form of pulse agility involving FM noise waveforms provides tremendous flexibility and design freedom to realize physical emissions for multiple different radar applications. The design of such waveforms tends to involve random initialization followed by optimization according to the error between a waveform's spectral content and a desired frequency-domain template. In contrast, here the spectral envelope is fixed and the optimization relies on the error relative to a desired temporal template (e.g. a constant amplitude pulse). It is demonstrated in simulation as well as experimentally in loopback that this temporal template error (TTE) approach provides sidelobe and spectral containment performance that is generally superior to previous frequency template forms and other FM noise design schemes.**

Keywords—waveform diversity, FM noise, pulse agility

I. INTRODUCTION

By definition, FM noise waveforms [1,2] require the temporal envelope to be constant amplitude, with this property being achieved through either an implicit or explicit constraint in the design process. Such waveforms have been theoretically analyzed in [3-5] and techniques have been developed to design practical versions for various purposes such as simultaneous dual-polarized operation [6], transmit spectral notching [7,8], nonlinear harmonic radar based on intermodulation of unique waveform pairs [9], a form of MIMO involving random spatial modulation that mimics the human eye [10], joint radar and communication waveforms [11], and even the experimental demonstration of practical waveforms having complementary attributes [12]. Further, note that this notion of "FM noise" follows the structure considered in [3-5] where the signal strictly remains FM (and could be implemented via [13]), as opposed to the similar terminology of [14,15] that rather differently involves the random fast-time perturbation of a linear FM (LFM) waveform in terms of phase and amplitude.

In contrast to many of the above FM noise design approaches, here we relax the constant amplitude constraint until the very end of the optimization process. More specifically, where the previous methods generally imposed a constant amplitude constraint (implicitly or explicitly) in the time domain while optimizing in terms of frequency domain error, the new temporal template error (TTE) approach conversely imposes a frequency content constraint while optimizing in terms of this time domain metric. The TTE formulation, which is solved via iterative gradient descent optimization, can thus be viewed as a hybridization of the frequency template error (FTE) approach [7,16] and pseudo-random optimized FM (PRO-FM) design of [1,2], where the former employs gradient descent and the latter uses projections.

It is shown that TTE-based gradient descent is able to obtain waveforms that have exactly the desired spectral characteristics and are nearly constant amplitude. Additionally, it is shown that the distortion imposed upon the desired spectrum by the final constant amplitude projection is quite minimal, so that the resulting FM noise waveforms achieve both good autocorrelation sidelobes and spectral containment compared to previous FM noise design approaches.

II. TEMPORAL TEMPLATE ERROR (TTE)

Define an arbitrary waveform in the frequency domain according to

$$S(f) = B(f)\exp(j\phi(f)), \tag{1}$$

where $B(f)$ is some desired spectral shape and $\phi(f)$ is an arbitrary phase function. In general, defining a waveform in this manner results in a time domain representation $s(t)$ that has a rather high peak-to-average power ratio (PAPR), which is clearly problematic for use with the high power amplifier (HPA) typical of most radar applications [17], and an extensive pulse width that may not even be finite (theoretically). Consequently, when defining a waveform in terms of (1) is likewise necessary to impose the desirable time-domain characteristics. With this requirement in mind, consider the TTE metric

$$J = \int_0^T \Big[|s(t)|^2 - u(t) \Big]^2 dt \tag{2}$$

in which $u(t)$ is the real-valued time-domain envelope of the desired pulse shape and

$$s(t) = \mathcal{F}^{-1}\{B(f)\exp(j\phi(f))\}, \tag{3}$$

for $\mathcal{F}^{-1}$ the inverse Fourier transform.

The metric in (2) measures squared error between the time-domain envelope of $s(t)$ and the desired envelope $u(t)$, where the latter has support on $[0, T]$ for T the desired pulse width. An interesting consideration here is whether or not to extend the integral in (2) over the entire time support of a given waveform $s(t)$, which in theory could extend over $(-\infty, +\infty)$, since this region would likewise contribute to the error. However, if $s(t)$ and $u(t)$ are each normalized to have the same energy, then any non-zero components of $s(t)$ outside of $[0, T]$ likewise incurs a difference between $s(t)$ and $u(t)$ within $[0, T]$ as well. Thus minimizing (2) implicitly minimizes the error outside $[0, T]$, making integration over $(-\infty, +\infty)$ unnecessary.

Our goal is therefore to minimize (2) via determination of $\phi(f)$, for which many possible solutions exist, thereby

This work was supported by the Office of Naval Research under Contract #N00014-16-C-2029. DISTRIBUTION STATEMENT A. Approved for Public Release.

providing many potential FM noise waveforms. Doing so is accomplished by first discretizing (2) as

$$J = \left\| \overline{\mathbf{s}}^{*} \odot \overline{\mathbf{s}} - \overline{\mathbf{u}} \right\|^2, \tag{4}$$

where

$$\overline{\mathbf{s}} = [\mathbf{s}^T \ \mathbf{0}_{1\times(M-1)}]^T \tag{5}$$

and

$$\overline{\mathbf{u}} = [\mathbf{u}^T \ \mathbf{0}_{1\times(M-1)}]^T \tag{6}$$

are zero-padded versions of the length-M vectors $\mathbf{s}$ and $\mathbf{u}$, which are in turn discretized versions of waveform $s(t)$ and temporal template $u(t)$, respectively, and $\|\cdot\|^2$ is the squared Euclidean norm. The zero padding has no effect on the actual value of (4), but is included to simplify the notation of the gradient.

The independent variables in (4) are thus the length $2M-1$ vector of phase values in $\boldsymbol{\phi}$, corresponding to the discretized version of the waveform spectrum of (1) as

$$\mathbf{s}_{\mathrm{f}} = \mathbf{b} \odot \exp(j\boldsymbol{\phi}), \tag{7}$$

which also has length $2M-1$ and with the additional $M-1$ samples needed to represent the autocorrelation of $\mathbf{s}$ (via inverse Fourier transform of (7)) without aliasing. The vector $\mathbf{b}$ in (7) is likewise the discretized representation of $B(f)$ from (1).

Finally, a length $2M-1$ time-domain representation of the waveform is realized via

$$\tilde{\mathbf{s}} = \mathbf{A}\mathbf{s}_{\mathrm{f}}, \tag{8}$$

where $\mathbf{A}$ is the $(2M-1)\times(2M-1)$ inverse discrete Fourier transform (IDFT) matrix and the first M samples of $\tilde{\mathbf{s}}$ correspond to the time interval $[0, T]$. Thus $\mathbf{s}$ is obtained by applying the function

$$\mathcal{Z}_N\{\tilde{\mathbf{s}}\} = \overline{\mathbf{s}} \tag{9}$$

where the operator $\mathcal{Z}_N\{\bullet\}$ replaces all samples after the Nth sample with zero. While there is almost certainly to be non-zero terms within the last $M-1$ samples that are nullified by $\mathcal{Z}_N\{\bullet\}$, the minimization of (4) implicitly minimizes the energy in this region as well.

III. Temporal Template Error Optimization

Due to the non-linearity of (4) with respect to $\boldsymbol{\phi}$, it is necessary to use numerical optimization techniques to minimize J. For parameterized waveform design such as discussed above, gradient techniques can be quite effective. Here we employ heavy ball gradient descent [18] as it has been found to provide a good tradeoff between convergence speed, numerically stability, and computational complexity. In this context the search direction at the kth iteration is

$$\mathbf{p}_k = \begin{cases} -\boldsymbol{g}_0 & \text{when } k = 0 \\ -\boldsymbol{g}_k + \beta \mathbf{p}_{k-1} & \text{otherwise} \end{cases}, \tag{10}$$

where $\mathbf{g}_k$ is the current gradient and $0 \le \beta \le 1$ is the heavy ball parameter. If $\mathbf{p}_k$ is ever found to actually be an ascent direction, it can be reset to $-\mathbf{g}_k$. With a search direction determined, the parameter vector update is computed as

$$\boldsymbol{\phi}_{k+1} = \boldsymbol{\phi}_k + \mu_k \mathbf{p}_k \tag{11}$$

where the current step size μ_k is chosen using a simple backtracking line search [19].

For any gradient descent method, the most important calculation, and often the computational bottleneck, is determination of the gradient itself. Consequently, (4) has been constructed such that the resulting gradient can be calculated using only matrix-vector operations and fast Fourier transforms (FFTs). A similar approach was used in [7,12,20,21]. In fact, the TTE metric can viewed as a "dual" to the frequency template error (FTE) metric evaluated in [7], in that the formulation and computational structures are the same, just with the domains switched and different independent variables.

It can be shown that the gradient of (4) with respect to frequency-domain phase vector $\boldsymbol{\phi}$ is

$$\mathbf{g} = \nabla_{\boldsymbol{\phi}} J = \frac{2}{J} \Im\left\{ \mathbf{s}_{\mathrm{f}} \odot \left[\mathbf{A}^H \left(\left\{ \overline{\mathbf{s}}^{*} \odot \overline{\mathbf{s}} - \overline{\mathbf{u}} \right\} \odot \overline{\mathbf{s}} \right) \right] \right\}, \tag{12}$$

where $\Im\{\bullet\}$ extracts the imaginary part of the argument. In other words, at the kth iteration $\mathbf{g}_k$ is dependent on $\mathbf{s}_k$ and $\mathbf{s}_{\mathrm{f},k}$, which in turn are both functions of $\boldsymbol{\phi}_k$.

In practice, minimizing (4) will not result in a perfect template match to $\mathbf{u}$, which has a constant amplitude envelope and is strictly limited in time to the interval $[0, T]$. Thus the final step in the optimization process is to project the discretized waveform onto the desired temporal envelope. Denoting $\hat{\mathbf{s}}$ as the length-M gradient-descent result, this projection is performed via

$$\mathbf{s} = \mathbf{u} \odot \exp(j\angle\hat{\mathbf{s}}), \tag{13}$$

where $\angle$ extracts the phase of the argument. This projection will always distort the desired spectrum $\mathbf{b}$. However, $\hat{\mathbf{s}}$ should already be very "close" to $\mathbf{u}$ in a squared-error sense, and thus the distortion should be minimal.

IV. Simulation Results

Compared to other FM noise waveform optimization techniques [1-12], the combination of gradient-descent with a projection is unique. Accordingly, we first assess how the projection affects the final optimized waveform before considering how the overall performance of optimized sets of TTE waveforms compares to other FM noise waveforms.

A. Projection Distortion Assesment

To demonstrate how minimizing the cost function affects the time-domain envelope, consider the initial and optimized envelopes of a single random waveform, with gradient descent performed for 10,000 iterations. The initial waveform was defined in the spectral domain to have a time-bandwidth product BT of 300 and a Gaussian spectrum that is over-sampled by 3 relative to 3-dB bandwidth. The Gaussian spectrum was chosen to take advantage of fact that the inverse Fourier transform of a Gaussian is another Gaussian, and so the

resulting autocorrelation theoretically has no sidelobes. The desired envelope **u** is constant amplitude and the frequency-domain phase was randomly initialized with each sample drawn from a uniform distribution on $[-\pi, +\pi]$.

The initial time envelope in Fig. 1 (blue) is clearly far from constant amplitude, though Fig. 2 shows that prior to projection onto **u** this signal does have a perfect Gaussian spectral shape based on (7). On the other hand, the optimized time envelope in Fig. 1 (orange) is much closer to the desired **u**, with a small amount of energy leakage beyond the end of the pulse width. Prior to projection, the optimized spectrum in Fig. 2 likewise has a perfect Gaussian shape via (7). However, once these initial and optimized versions of the waveform are projected onto the desired envelope **u** it is observed in Fig. 2 that the latter retains a spectrum that is much closer to the desired Gaussian power spectrum than the former because the optimized time-domain envelope is already quite close to **u**. This anecdotal result confirms the operating assumption that, by finding a signal with a desired spectrum that has a temporal envelope close to the desired form, subsequent forcing onto the desired temporal envelope only slightly distorts the desired spectrum.

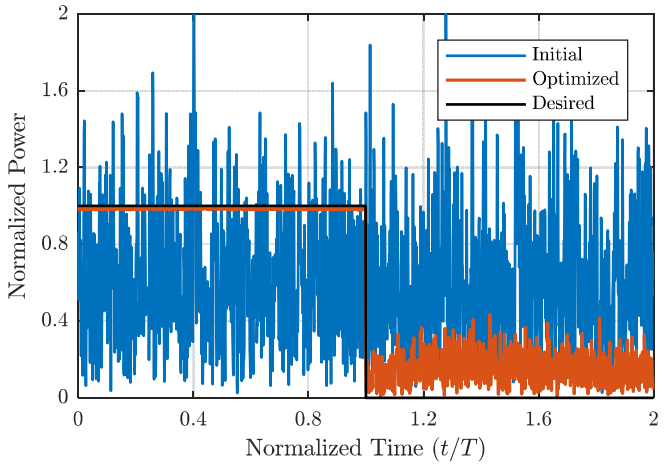

Fig. 1. Temporal envelopes of initial and TTE-optimized random waveforms before projection onto the desired envelope **u**

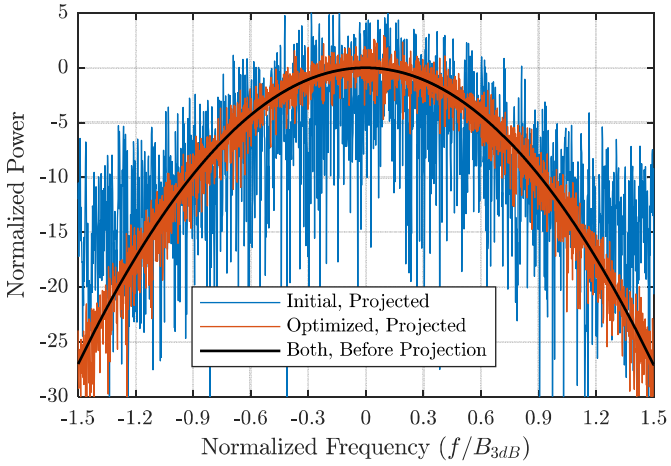

Fig. 2. Power spectra of initial and TTE-optimized random waveforms before and after being projected onto the desired time envelope **u**

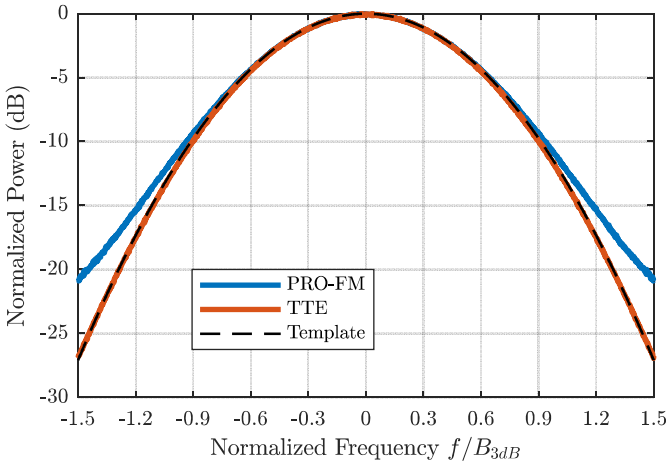

Fig. 3. Mean power spectra of 1000 PRO-FM and TTE waveforms compared to the desired spectrum with 3× oversampling (relative to 3-dB bandwidth)

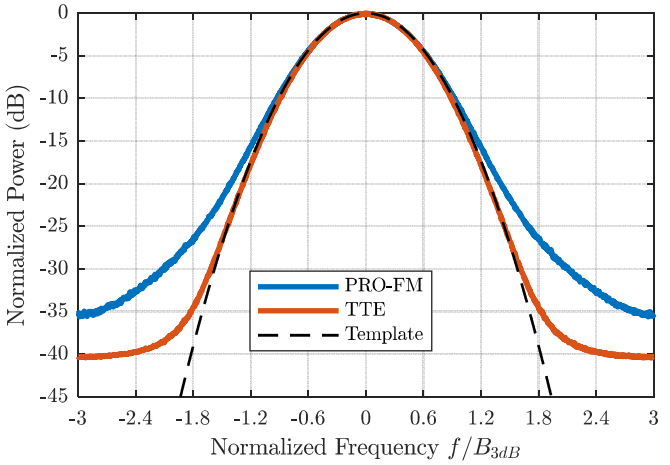

Fig. 4. Mean power spectra of 1000 PRO-FM and TTE waveforms compared to the desired spectrum with 6× oversampling (relative to 3-dB bandwidth)

B. TTE Optimization Performance

Using the same parameters as the waveform in Figs. 1 and 2, the TTE formulation was used to optimize 1000 random FM waveforms. As a point of comparison, 1000 pseudo-random optimized (PRO-FM) waveforms were also optimized according to [2] to have the same Gaussian spectrum using the same oversampling factor and time-bandwidth product.

In Fig. 3, the mean power spectra of all 1000 TTE and PRO-FM waveforms (with an oversampling factor of 3) are plotted against the desired Gaussian spectrum. Throughout the waveform passband, which corresponds to the normalized frequency interval from −0.5 to +0.5, both approaches do an excellent job of matching the desired spectral template. Below a normalized power of −10 dB (normalized frequency of ±0.9), however, the PRO-FM mean spectrum begins to deviate from the template, leading to worse spectral containment relative to the TTE case.

In Fig. 4 the mean spectra of these waveform sets are plotted with an oversampling factor of 6. The passband template match is still excellent, but beyond a normalized frequency of about ±1.2 (below −15 dB), the PRO-FM spectrum again deviates

from the template. It is observed here that the TTE spectral likewise deviates from the template, albeit not until a normalized frequency of about ±1.6 (or below −30 dB). The TTE spectrum also flattens out at roughly −40 dB, which is quite similar to what was found for the Log-FTE metric in [7] and is likely caused by the spectral content of the sharp rise/fall of the pulse edges.

Figures 5 and 6 show the integrated autocorrelations (over each set of 1000 waveforms) associated with Figs. 3 and 4, respectively, which is also corresponds to the zero-Doppler response if these 1000 waveforms comprised a coherent processing interval (CPI). Despite the differences in the spectral roll-off of these waveforms, there is little qualitative difference between their autocorrelation responses.

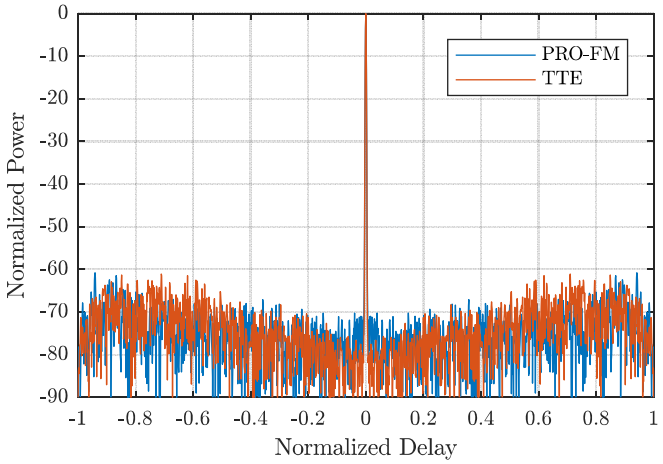

Fig. 5. Integrated (coherently summed across pulses) autocorrelations of 1000 PRO-FM and TTE waveforms (3× oversampling)

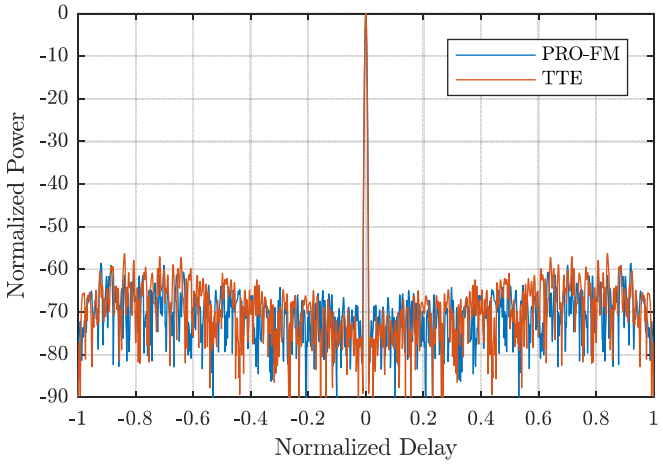

Fig. 6. Integrated (coherently summed across pulses) autocorrelations of 1000 PRO-FM and TTE waveforms (6× oversampling)

V. Experimental Results

To illustrate the utility of these waveforms in practice, the TTE and PRO-FM optimized waveforms in the previous section were each captured in loopback and used to collect open-air measurements.

A. Loopback Assesment

From a baseband sample rate of 200 MSample/sec each waveform was up-sampled to 10 GSample/sec and then digitally up-converted to a center frequency of 3.55 GHz. The signals were then produced by a Tektronix AWG70002A arbitrary waveform generator (AWG) with a 10-bit depth, passed through a class-A amplifier and then an attenuator. They were then captured in the "receiver" where they were amplified by an LNA to approximate a real, open-loop configuration. The signals were recorded using a Rhode & Schwarz FSW real time spectrum analyzer (RSA).

Figures 7 and 8 are the loopback versions of the waveform mean spectra depicted in Figs. 3 and 4. Comparing them, the most noticeable effect is the steep roll-off induced by the anti-aliasing filter of the RSA "receiver". Otherwise, the spectra below the RSA filter cutoff is relatively unaffected. Considering the limited spectral distortion observed in Figs. 7 and 8, it is therefore unsurprising how well the loopback integrated autocorrelations in Figs. 9 and 10 likewise match there simulated counterparts in Figs. 5 and 6. In short, all the waveforms were implemented in loopback with relatively little distortion compared to their simulated counterparts.

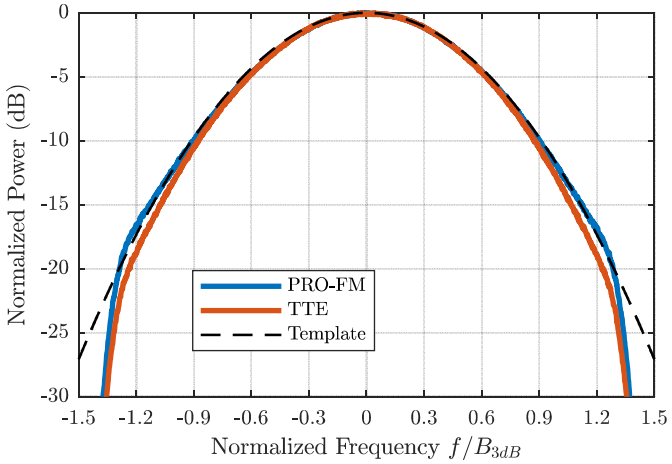

Fig. 7. Mean power spectra of 1000 PRO-FM and TTE waveforms measured in loopback compared to the desired spectrum (3× oversampling)

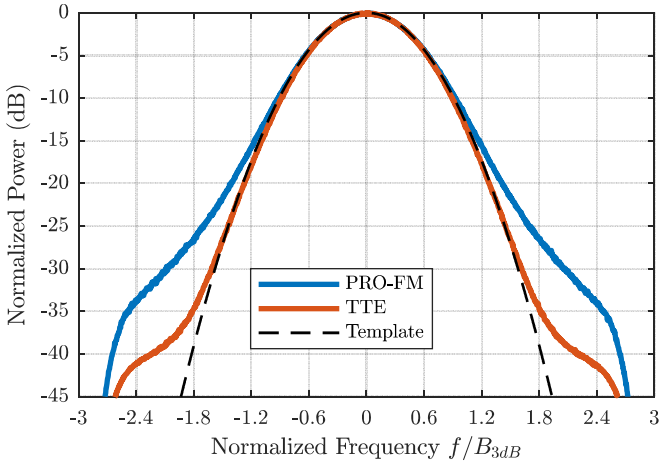

Fig. 8. Mean power spectra of 1000 PRO-FM and TTE waveforms measured in loopback compared to the desired spectrum (6× oversampling)

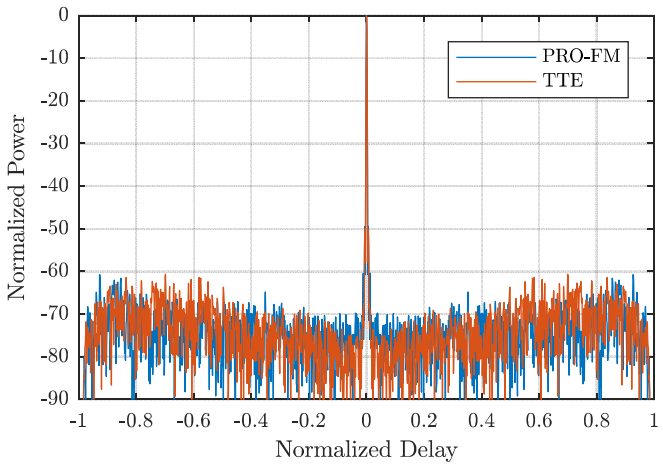

Fig. 9. Integrated (coherently summed across pulses) autocorrelations of 1000 PRO-FM and TTE waveforms captured in loopback (3× oversampling)

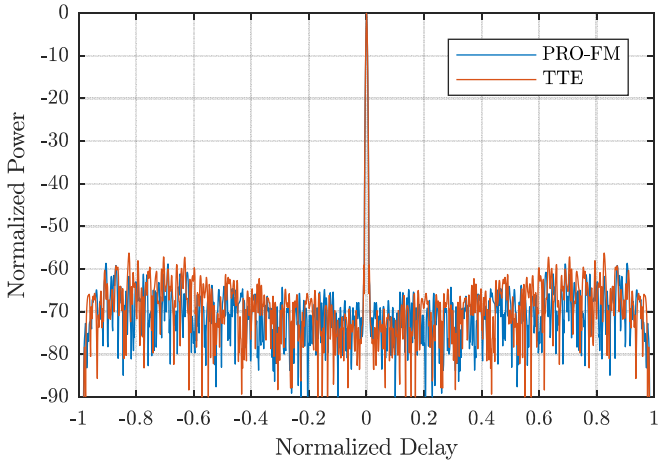

Fig. 10. Integrated (coherently summed across pulses) autocorrelations of 1000 PRO-FM and TTE waveforms captured in loopback (6× oversampling)

A. Open-Air Measurements

To further validate the performance of the TTE waveforms, they were transmitted from the rooftop of Nichols Hall at the University of Kansas towards the intersection of 23rd and Iowa streets in Lawrence, KS. Given the up-sampled waveform parameters, the bandwidth of B = 66.7 MHz results in a range resolution of 2.5 m. The pulse repetition frequency was set to 20 kHz, thus providing a CPI of 50 ms (for 1000 waveforms) which corresponds to a velocity resolution of 0.85 m/s.

In Fig. 11, the range profile (zero Doppler cut) generated by each set of waveforms is plotted. Of particular interest are the sidelobe levels of the direct path, which are clearly evident in the "negative range" portion of Fig. 11. The negative range occurs because this area represents the convolutional tails of the matched filtering. In this region, the sidelobe levels of both the PRO-FM and TTE waveforms are relatively level with each other. Given the similarity in the loopback results of the PRO-FM and the TTE waveforms, the similarity between their range profiles here is unsurprising. That said, some small differences (e.g. at 0.6 km) are visible.

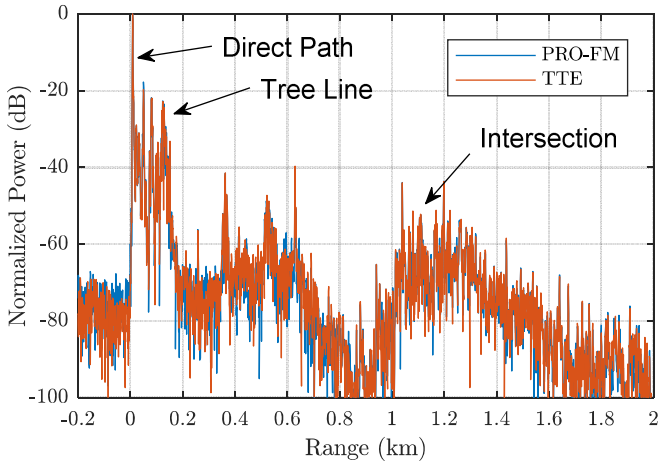

Fig. 11. Measured range profile for both the 3 times oversampled PRO-FM and TTE waveforms

In Figs. 12 and 13 range-Doppler responses for the PRO-FM and TTE waveforms are plotted, respectively, after applying a Hamming window to suppress Doppler sidelobes and performing clutter cancellation based on a simple zero-Doppler projection (since the platform is stationary). In the interest of collecting a large number of movers, the transmit test was timed such that there were several cars moving through the intersection at the time (i.e. just after a light change). Additionally, the waveform sets were transmitted back to back to facilitate illumination very similar scenes for comparison.

Numerous moving targets are visible in both cases, thus demonstrating the ability of TTE waveforms to perform at least as well as PRO-FM waveforms for MTI applications. Further, there are no range sidelobes visible in either case because the 45 dB dynamic range observed in this scenario is less than the 60 dB peak to sidelobe ratio observed in Figs. 9 and 10. In any case, like many of the FM noise waveforms before it, TTE waveforms are clearly robust to physical implementation and provide advantages with regard to spectral containment. In fact, it is been found (though not shown here) that this improved spectral containment also translates into some degree of improved robustness against transmitter distortion effects due to their being less impacted by the natural bandlimiting of the transmitter.

VI. Conclusions

The temporal template error (TTE) cost function was defined and minimized using gradient descent as a new means to optimize FM noise waveforms. The TTE optimization additionally employs a final time-domain projection step to force waveforms to match a particular temporal envelope, such as that of a constant amplitude pulse. Despite the inevitable spectral distortion imparted by this projection, the TTE optimized waveforms were shown in simulation, experimentally in loopback, and through open-air testing to achieve comparable autocorrelation sidelobe levels and improved spectral containment relative to previously developed FM noise waveforms.

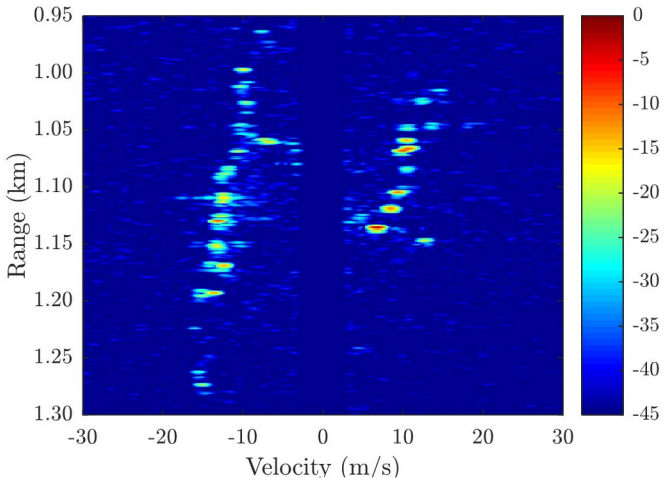

Fig. 12. Range-Doppler response for PRO-FM waveforms (3× oversampling)

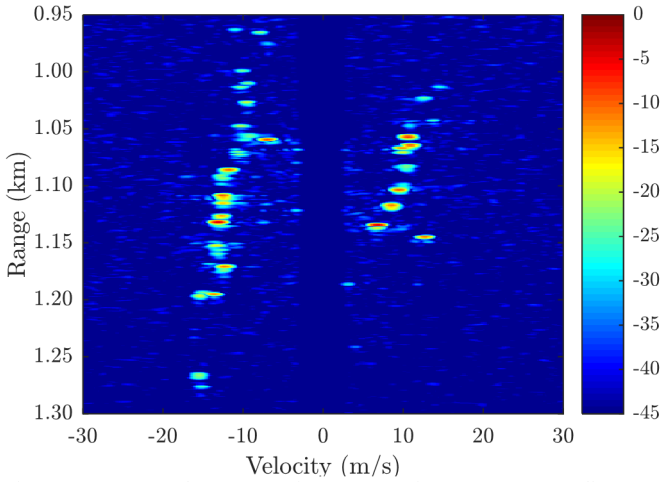

Fig. 13. Range-Doppler response for TTE waveforms (3× oversampling)

REFERENCES

[1] J. Jakabosky, S.D. Blunt, B. Himed, "Waveform design and receive processing for nonrecurrent nonlinear FMCW radar," *IEEE Intl. Radar Conf.*, Arlington, VA, May 2015.

[2] J. Jakabosky, S. D. Blunt, B. Himed, "Spectral-shape optimized FM noise radar for pulse agility," *IEEE Radar Conf.*, Philadelphia, PA, May 2016.

[3] S.R.J. Axelsson, "Noise radar using random phase and frequency modulation," *IEEE Trans. Geoscience & Electronic Systems*, vol. 42, no. 11, pp. 2370-2384, Nov. 2004.

[4] L. Pralon, G. Beltrao, B. Pompeo, M. Pralon, J.M. Fortes, "Near-thumbtack ambiguity function of random frequency modulated signals," *IEEE Radar Conf.*, Seattle, WA, May 2017.

[5] L. Pralon, B. Pompeo, J.M. Fortes, "Stochastic analysis of random frequency modulated waveforms for noise radar systems," *IEEE Trans. Aerospace & Electronic Systems*, vol. 51, no. 2, pp. 1447-1461, Apr. 2015.

[6] G. Zook, P.M. McCormick, S.D. Blunt, C. Allen, J. Jakabosky, "Dual-polarized FM noise radar," *IET International Conference on Radar Systems*, Belfast, UK, Oct. 2017.

[7] C. A. Mohr, P. M. McCormick, S. D. Blunt, C. Mott, "Spectrally-efficient FM noise radar waveforms optimized in the logarithmic domain," *IEEE Radar Conf.*, Oklahoma City, OK, Apr. 2018.

[8] B. Ravenscroft, J.W. Owen, J. Jakabosky, S.D. Blunt, A.F. Martone, K.D. Sherbondy, "Experimental demonstration and analysis of cognitive spectrum sensing & notching," *IET Radar, Sonar & Navigation*, vol. 12, no. 12, pp. 1466-1475, Dec. 2018.

[9] J. Owen, S.D. Blunt, K. Gallagher, P. McCormick, C. Allen, K. Sherbondy, "Nonlinear radar via intermodulation of FM noise waveform pairs," *IEEE Radar Conf.*, Oklahoma City, OK, Apr. 2018.

[10] G. Zook, P. McCormick, S.D. Blunt, "Fixational eye movement radar: random spatial modulation," *IEEE Radar Conf.*, Oklahoma City, OK, Apr. 2018.

[11] B. Ravenscroft, P.M. McCormick, S.D. Blunt, E. Perrins, J.G. Metcalf, "A power-efficient formulation of tandem-hopped radar & communications," *IEEE Radar Conf.*, Oklahoma City, OK, Apr. 2018.

[12] C. A. Mohr, P. M. McCormick, S. D. Blunt, "Optimized complementary waveform subsets within an FM noise radar CPI," *IEEE Radar Conf.*, Oklahoma City, OK, Apr. 2018.

[13] S.D. Blunt, M. Cook, J. Jakabosky, J. de Graaf, and E. Perrins, "Polyphase-coded FM (PCFM) radar waveforms, part I: implementation," *IEEE Trans. Aerospace & Electronic Systems*, vol. 50, no. 3, pp. 2218-2229, July 2014.

[14] M.A. Govoni, H. Li, J.A. Kosinski, "Range-Doppler resolution of the linear-FM noise radar waveform," *IEEE Trans. Aerospace & Electronic Systems*, vol. 49, no. 1, pp. 658-664, Jan. 2013.

[15] M.A. Govoni, H. Li, J.A. Kosinski, "Low probability of interception of an advanced noise radar waveform with linear-FM," *IEEE Trans. Aerospace & Electronic Systems*, vol. 49, no. 2, pp. 1351-1356, Apr. 2013.

[16] S.D. Blunt, J. Jakabosky, M. Cook, J. Stiles, S. Seguin, E.L. Mokole, "Polyphase-coded FM (PCFM) radar waveforms, part II: optimization," *IEEE Trans. Aerospace & Electronic Systems*, vol. 50, no. 3, pp. 2230-2241, July 2014.

[17] S.D. Blunt, E.L. Mokole, "An overview of radar waveform diversity," *IEEE AESS Systems Magazine*, vol. 31, no. 11, pp. 2-42, Nov. 2016.

[18] E. Ghadimi, R. Feyzmahdavian, M. Johansson, "Global convergence of the heavy-ball method for convex optimization," *European Control Conf.*, Linz, Austria, July 2015.

[19] J. Nocedal, S. Wright. *Numerical Optimization*, Springer Science & Business Media, 2006.

[20] B. O'Donnell, J.M. Baden, "Fast gradient descent for multi-objective waveform design," *IEEE Radar Conf.*, Philadelphia, PA, May 2016.

[21] D. Zhao, Y. Wei, Y. Liu, "Spectrum optimization via FFT-based conjuage gradient method for unimodular sequence design," *Signal Processing*, vol. 142, pp. 354-365, Jan. 2018.